LETTERS

Observation of unidirectional backscattering-immune topological electromagnetic states

Zheng Wang[1]*, Yidong Chong[1]†*, J. D. Joannopoulos[1] & Marin Soljačić[1]

One of the most striking phenomena in condensed-matter physics is the quantum Hall effect, which arises in two-dimensional electron systems[1–4] subject to a large magnetic field applied perpendicular to the plane in which the electrons reside. In such circumstances, current is carried by electrons along the edges of the system, in so-called chiral edge states (CESs). These are states that, as a consequence of nontrivial topological properties of the bulk electronic band structure, have a unique directionality and are robust against scattering from disorder. Recently, it was theoretically predicted[5–7] that electromagnetic analogues of such electronic edge states could be observed in photonic crystals, which are materials having refractive-index variations with a periodicity comparable to the wavelength of the light passing through them. Here we report the experimental realization and observation of such electromagnetic CESs in a magneto-optical photonic crystal[7] fabricated in the microwave regime. We demonstrate that, like their electronic counterparts[8–13], electromagnetic CESs can travel in only one direction and are very robust against scattering from disorder; we find that even large metallic scatterers placed in the path of the propagating edge modes do not induce reflections. These modes may enable the production of new classes of electromagnetic device and experiments that would be impossible using conventional reciprocal photonic states alone. Furthermore, our experimental demonstration and study of photonic CESs provides strong support for the generalization and application of topological band theories to classical and bosonic systems, and may lead to the realization and observation of topological phenomena in a generally much more controlled and customizable fashion than is typically possible with electronic systems.

The existence of photonic CESs was first predicted[5,6] by an analogy between a photonic crystal[14–16] with broken time-reversal symmetry and a system exhibiting the quantum Hall effect (QHE). In this analogy, the electromagnetic fields play the part of the electronic current, the variations of permittivity and permeability within the photonic crystal play the part of the periodic potential and the gradients of the gyrotropic components of the permeability tensor play the part of the external d.c. magnetic field that breaks the time-reversal symmetry[5–7]. The defining feature of a photonic CES is that its group velocity points in only one direction, which is determined by the sign of the field that breaks the time-reversal symmetry and the resulting unusual topological properties of the bulk band structure. To detect the possible presence of non-trivial topological band properties in a photonic-crystal system it is sufficient[5–7] to compute its Chern numbers. (Although the original proposal[5,6] focused on 'Dirac points', it is not necessary to restrict to such band structures; thus, the use of a variety of photonic-crystal systems is possible[7].) The Chern number of band n of a two-dimensional (2D) periodic photonic crystal is an integer defined by[6]

$$C_n = \frac{1}{2\pi i} \int_{\mathrm{BZ}} \mathrm{d}^2 k \left(\frac{\partial A_y^{nn}}{\partial k_x} - \frac{\partial A_x^{nn}}{\partial k_y} \right)$$

where the k-space integral is performed over the first Brillouin zone and the Berry connection[6] is given by

$$\mathbf{A}^{nn'}(\mathbf{k}) \equiv i\langle \mathbf{E}_{n\mathbf{k}} | \nabla_{\mathbf{k}} | \mathbf{E}_{n'\mathbf{k}} \rangle = i \int \mathrm{d}^2 r \varepsilon(\mathbf{r}) \mathbf{E}^*_{n\mathbf{k}}(\mathbf{r}) \cdot [\nabla_{\mathbf{k}} \mathbf{E}_{n'\mathbf{k}}(\mathbf{r})]$$

where $\mathbf{E}_{n\mathbf{k}}$ is the periodic part of the electric-field Bloch function[16], an asterisk denotes complex conjugation and $\varepsilon(\mathbf{r})$ denotes the dielectric function. Because the Chern number characterizes the winding number of the phase of the Bloch functions around the boundary of the first Brillouin zone[11], it is a 'global' or 'topological' property of the entire band and is very robust against structural perturbations[10]. Notably, it can be non-zero only if the system lacks time-reversal symmetry[9].

One of the most interesting properties of QHE systems is that the Chern numbers have a direct physical significance: a finite crystal that supports bulk bands with non-zero Chern numbers also supports unidirectional CESs at its boundary at energies within bulk band gaps opened by the applied d.c. magnetic field. Moreover, the number of CESs turns out to be equal to the sum of the Chern numbers of all the bulk bands of lower energy[13]. Although this result has been formally proven only in a tight-binding QHE system, it is believed to be independent of the details of the underlying model, such as the structure of the lattice and the edge. Its validity in photonic-crystal systems was originally predicted in refs 5, 6, and corroborated through a formal mapping[7] to a 'zero-field QHE' system[12] and *ab initio* numerical simulations of Maxwell's equations[7]. It is important to emphasize that although CESs have so far been experimentally observed only in electronic (that is, fermionic) systems, the phenomenon should actually be independent of the underlying particle statistics because the Chern number is defined in terms of single-particle Bloch functions. An experimental verification would therefore provide strong support for the generalization of topological band theories and their applications to classical and bosonic systems.

The ability to work with photonic-crystal band structures without Dirac points has allowed us to design an experimentally viable photonic-crystal system[7] for the observation of CESs. Our experimental system (Fig. 1) involves a gyromagnetic, 2D-periodic photonic crystal consisting of a square lattice of ferrite rods in air (details of the structure and materials used can be found in Methods), bounded on one side by a non-magnetic metallic cladding. The interface between the photonic crystal and the cladding acts as a confining edge or waveguide for CESs. (Without this cladding, the CESs at the air edges of the photonic crystal would simply radiate away.) Neglecting absorption losses and nonlinear effects, we would expect power transmission of a CES along this waveguide to be independent of the waveguide geometry and also immune to backscattering from disorder, obstacles and defects.

[1]Department of Physics, Massachusetts Institute of Technology, Cambridge, Massachusetts 02139, USA. †Present address: Yale University, New Haven, Connecticut 06520, USA.
*These authors contributed equally to this work.

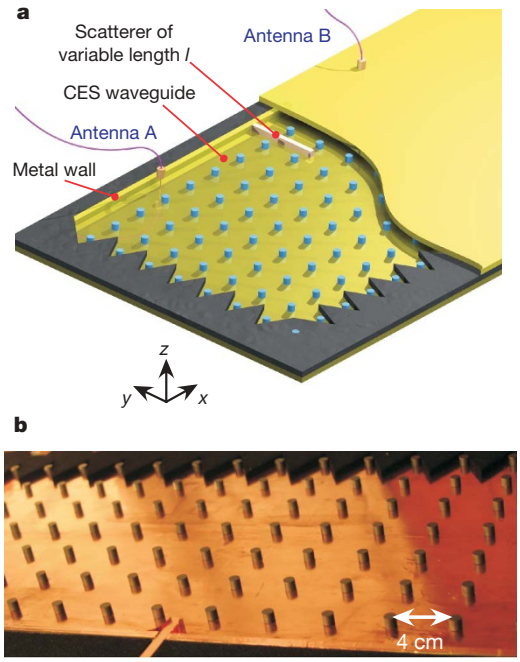

Figure 1 | Microwave waveguide supporting CESs. a, Schematic of the waveguide composed of an interface between a gyromagnetic photonic-crystal slab (blue rods) and a metal wall (yellow). The structure is sandwiched between two parallel copper plates (yellow) for confinement in the *z* direction and surrounded with microwave-absorbing foams (grey regions). Two dipole antennas, A and B, serve as feeds and/or probes. A variable-length (*l*) metal obstacle (orange) with a height equal to that of the waveguide (7.0 mm) is inserted between the antennas to study scattering. A 0.20-T d.c. magnetic field is applied along the *z* direction using an electromagnet (not shown). **b**, Top view (photograph) of the actual waveguide with the top plate removed.

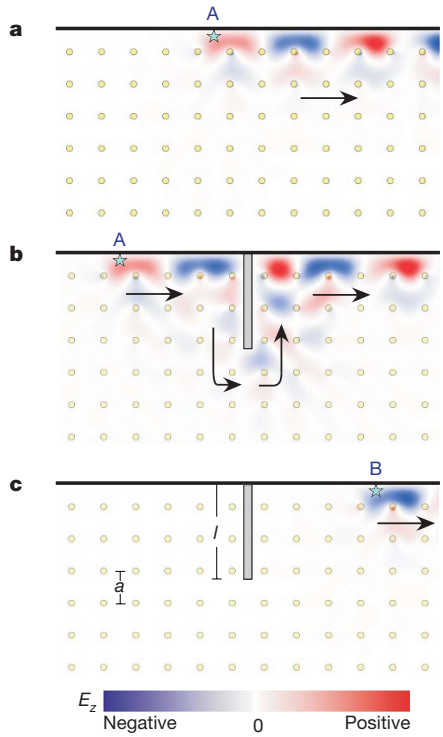

Figure 2 | Photonic CESs and effects of a large scatterer. a, CES field distribution (E_z) at 4.5 GHz in the absence of the scatterer, calculated from finite-element steady-state analysis (COMSOL Multiphysics). The feed antenna (star), which is omnidirectional in homogeneous media (Supplementary Information), radiates only to the right along the CES waveguide. The black arrow represents the direction of the power flow. **b**, When a large obstacle (three lattice constants long) is inserted, forward transmission remains unchanged because backscattering and side-scattering are entirely suppressed. The calculated field pattern (colour scale) illustrates how the CES wraps around the scatterer. **c**, When antenna B is used as feed antenna, negligible power is transmitted to the left, as the backwards-propagating modes are evanescent. *a*, lattice constant.

Before we discuss the results of our measurements, we will first describe how we arrived at this particular choice of experimental system. We chose rods in air for the basic photonic-crystal geometry because of ease of fabrication. We then performed a series of numerical simulations for a variety of rod sizes and lattice constants on a model 2D photonic-crystal system to optimize the band structure and compute corresponding band Chern numbers using material parameters appropriate to a low-loss ferrite (Methods). Our numerical simulations predicted that when the ferrite rods in this photonic crystal are magnetized to manifest gyrotropic permeability (which breaks time-reversal symmetry), a gap opens between the second and third transverse magnetic (TM) bands. Moreover, the second, third and fourth bands of this photonic crystal acquire Chern numbers of 1, −2 and 1, respectively. This result follows from the C_{4v} symmetry of a non-magnetized crystal[17]. The results of our simulations for the photonic crystal with metallic cladding are presented in Fig. 2. (Similar numerical results were obtained in ref. 7, albeit using a different material system and geometry.) Here we show the calculated field patterns of a photonic CES residing in the second TM band gap (between the second and the third bands). Because the sum of the Chern numbers over the first and second bands is 1, exactly one CES is predicted to exist at the interface between the photonic crystal and the metal cladding. The simulations clearly predict that this photonic CES is unidirectional. As side-scattering is prohibited by the bulk photonic band gaps in the photonic crystal and in the metallic cladding, the existence of the CES forces the feed dipole antennas (which would radiate omnidirectionally in a homogeneous medium) to radiate only towards the right (Fig. 2a, c). Moreover, the lack of any backwards-propagating mode eliminates the possibility of backscattering, meaning that the fields can continuously navigate around obstacles, as shown in Fig. 2b. Hence, the scattering from the obstacle results only in a change of the phase (compare Fig. 2a and Fig. 2b) of the transmitted radiation, with no reduction in amplitude.

For CESs to be readily measurable in the laboratory (where it is necessary to use a photonic crystal of finite and manageable size) they must be spatially well localized, and this requires the photonic band gaps containing the states to be large. The sizes of the band gaps that contain CESs (and the frequencies at which they occur) are determined by the gyromagnetic constants of the ferrite rods constituting the photonic crystal. Under a d.c. magnetic field, microwave ferrites exhibit a ferromagnetic resonance at a frequency determined by the strength of the applied field[18]. Near this frequency, the Voigt parameter, $V = |\mu_{xy}|/|\mu_{xx}|$ (where μ_{xx} and μ_{xy} are diagonal and off-diagonal elements of the permeability tensor, respectively), which is a direct measure of the strength of the gyromagnetic effect, is of order one. Such ferromagnetic resonances are among the strongest low-loss gyrotropic effects at room temperature and subtesla magnetic fields. Using ferrite rods composed of vanadium-doped calcium–iron–garnet under a biasing magnetic field of 0.20 T (Methods and Supplementary Information), we achieved a relative bandwidth of 6% for the second TM band gap (around 4.5 GHz in Fig. 3b). As discussed earlier, this is the gap predicted to support a CES at the interface of the photonic crystal with the metallic wall. We emphasize again that band gaps with trivial topological properties (that is, for which the Chern numbers of the bulk bands of lower frequencies sum to zero), such as the first TM band gap (around 3 GHz in Fig. 3b), do not support CESs. All of the insight gained from the model 2D photonic-crystal system was then incorporated into the final design (Fig. 1). To emulate the states of the 2D photonic crystal, the final design

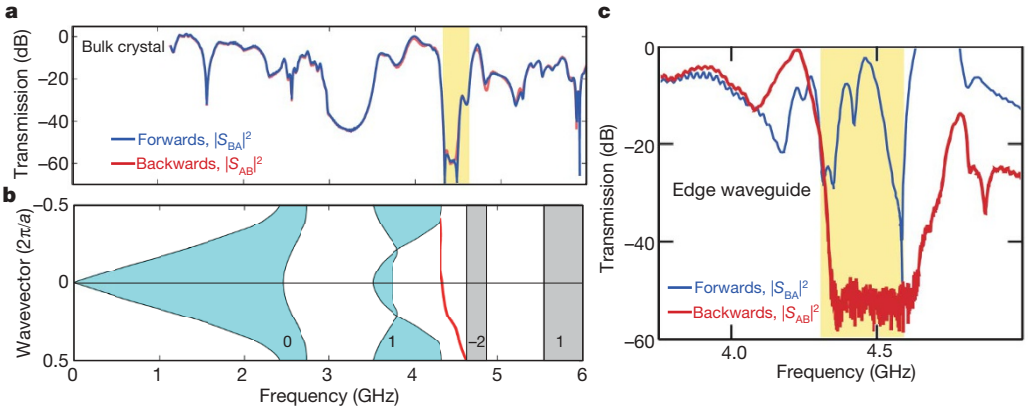

Figure 3 | CES-facilitated waveguiding in a photonic crystal. **a**, Forward and backward transmission spectra measured using only the bulk photonic crystal in the set-up shown in Fig. 1 (that is, without the metal cladding and obstacle), with the antennas placed in the interior of the photonic crystal, in a 0.20-T d.c. magnetic field. The bulk transmission is reciprocal, with photonic band gaps at 3.3 and 4.5 GHz. **b**, Calculated projected photonic-crystal band structure (blue and grey areas). Included is the CES (red curve) that exists at the interface between the metal cladding and the photonic crystal. The grey areas are bulk bands with ill-defined band-edges due to large absorption near the ferromagnetic resonance. Each band's Chern number is labelled. **c**, Measured transmission spectra upon inclusion of the metal cladding and antennas placed as shown in Fig. 1. In the resulting CES waveguide, there is very high contrast between the forward and backward transmissions for frequencies in the second band gap (yellow), around 4.5 GHz. This striking unidirectionality indicates the existence of a CES.

involved fabrication of a three-dimensional (3D) photonic-crystal slab structure equivalent to the model 2D photonic-crystal system, made from gyromagnetic rods with parallel metallic plates on the top and bottom, spaced to support only transverse electromagnetic modes (identical to the TM modes in the 2D photonic crystal; see Methods). A copper wall was then added at the edge of the photonic-crystal slab to provide the required cladding.

In our experiments, the band gaps and the CES waveguide were characterized using two-port vector network analysis using a pair of dipole antennas, labelled A and B in Fig. 1a (Methods). First, to characterize the band gap, we inserted antennas A and B into the interior of the photonic crystal far from the edges and eight lattice constants apart. We observed the second band gap with a 50-dB extinction for both forward and backward transmission (with respective transmission coefficients S_{BA} and S_{AB}; Fig. 3a). The frequency ranges of both the first and the second band gaps agree well with our predicted band structure calculations (no adjustable parameters; Fig. 3b). Next, to characterize the CESs, we measured the transmission spectra with the apparatus as illustrated in Fig. 1a (Methods). At frequencies within the second band gap, we observed a strong forward transmission, approximately 50 dB greater than the backward transmission at mid-gap frequencies (Fig. 3c). Over much of this frequency range, the backward transmission was below the noise floor of the network analyser, which suggests an even greater actual contrast. This difference of more than five orders of magnitude in power transmission, over a distance of only eight lattice constants, confirms that backwards-propagating modes are highly evanescent, as predicted.

We tested the robustness of the unidirectional propagation by studying the effect of a large obstacle on transmission. We gradually inserted a conducting barrier across the waveguide, blocking the direct path between antennas A and B. The measured transmission behaviour at different stages of the insertion (Fig. 4) remains basically the same as that in Fig. 3c: the transmission between 4.35 and 4.62 GHz remains strongly non-reciprocal, with a 40–50-dB difference between the forward and backward transmissions. This finding agrees with the theoretical prediction that power transmission by means of CESs is fundamentally insensitive to scattering from arbitrarily large defects (Fig. 2b). This behaviour is a distinguishing feature of the present waveguide. In a conventional waveguide, insertion of such a large obstacle would cause very large backscattering and significantly reduced transmission to the output. For example, in a photonic crystal constructed using ordinary dielectric rods and with identical dimensions (Supplementary Information), a similar barrier length of 1.65 lattice constants reduces forward transmission by four orders of magnitude. This measurement further confirms that the backwards-propagating modes are purely evanescent, and not merely lossy. If lossy backwards-propagating modes existed in the system, a large defect would scatter a significant portion of energy into them, essentially converting backscattering into loss. The forward transmission in the presence of the large defect would be much smaller than in

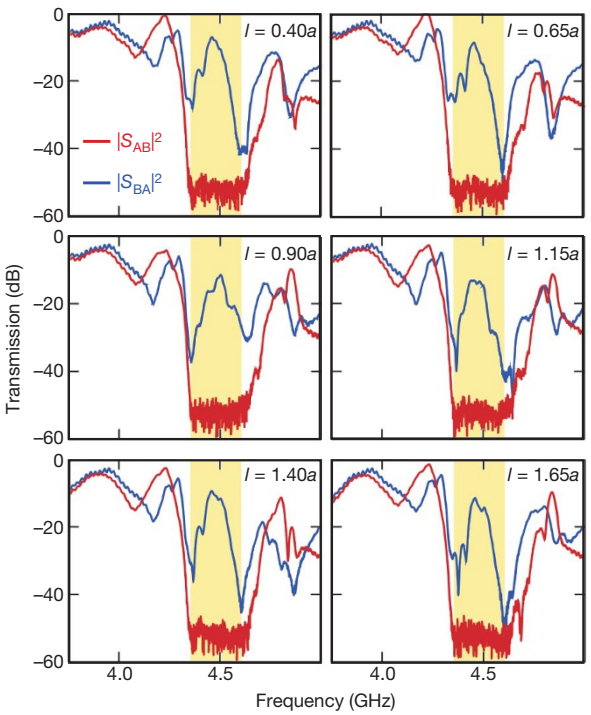

Figure 4 | CES transmission spectra in the presence of a large scatterer. The length of the obstacle, l, was gradually varied from 0.40a to 1.65a (lattice constant, a = 40 mm); this induced only minor differences in the forward transmission near the mid-gap frequency of 4.5 GHz. The lack of any significant changes in the forward transmission, and non-reciprocity ($|S_{AB}| \ll |S_{BA}|$) with large increases in the size of the scatterer, indicate that the CES can travel around the obstacle without scattering or reflections, as predicted by simulations. The experimental parameters remained unchanged from the measurement in Fig. 3c.

the defect-free case. Existing optical isolators, such as those relying on Faraday rotation or non-reciprocal phase shifts, absorb or radiate backwards-propagating light in this way. Thus, the unidirectional guiding of a CES is fundamentally different from how optical isolators operate.

The experimental establishment of topological photonic states opens a wide range of future opportunities. First, our realization of nontrivial topological Chern numbers in a classical photonic system raises the possibility of using photonic systems to realize other classes of topological quantum numbers that are of interest in condensed-matter physics. Examples include the Z_2 topological number associated with the quantum spin Hall effect[19–22] and the 'Hopf number' in certain 3D insulators[23]. Photonic crystals are attractive for such investigations because parameters such as lattice constants and unit-cell geometries can be chosen in a fully controlled manner[16], unlike in most electronic systems. Second, the fact that the CESs in the present system are immune to scattering from disorder ensures that the design is tolerant of fabrication imperfections, such as variations in the lattice constant or the exact position of the guiding edge; this could enable implementation of extremely robust waveguides. Finally, photonic CESs might prove useful in applications involving isolators[24] or slow light[25,26]. In conventional slow-light systems, disorder induces backscattering that increases quadratically with reduced group velocity[27], making them very sensitive to disorder. Although the experiments described here were conducted at gigahertz frequencies, this operating frequency can be increased simply by applying a stronger d.c. magnetic field[18]. Extension into the terahertz range might be achieved using metamaterials that resonantly enhance the magnetic activity[28–30]. Further extension to the optical regime is challenging, given the losses and weak gyrotropic effects in currently known materials.

METHODS SUMMARY

The gyromagnetic photonic crystal was constructed using a square array (lattice constant, $a = 40$ mm) of vanadium-doped calcium-iron-garnet (VCIG; TCI ceramics NG-1850) rods. Balancing the need for a large Voigt parameter against the drawback of absorption loss in the vicinity of the ferromagnetic resonance (5.6 GHz), we designed the rod radius to be 3.9 mm and a to be 40 mm to maximize the bandwidth of the band gap without suffering excessive loss. A 16×10 array was used to measure the band gap of a bulk crystal and a 16×7 array was used to study the waveguide and the effect of scattering. The VCIG ferrite has a measured relative permittivity of $\varepsilon_r = 14.63$ and a loss tangent of $\tan\delta = 0.00010$. The saturation magnetization was measured to be $M_s = 1.52 \times 10^5\ \mathrm{A\,m^{-1}}$, with a 3-dB linewidth of the ferromagnetic resonance at $\Delta H = 1.03 \times 10^3\ \mathrm{A\,m^{-1}}$. Using the cyclotron electromagnet at Massachusetts Institute of Technology, we applied a d.c. magnetic field of 0.20 T along the out-of-plane z direction, with a spatial non-uniformity of less than 1.5%. The d.c. magnetic field breaks the time-reversal symmetry in the photonic crystal. The magnetic field strength was measured and calibrated using a LakeShore Model 410 gaussmeter.

Full Methods and any associated references are available in the online version of the paper at www.nature.com/nature.

Received 1 June; accepted 15 July 2009.

1. von Klitzing, K., Dorda, G. & Pepper, M. New method for high-accuracy determination of the fine-structure constant based on quantized Hall resistance. *Phys. Rev. Lett.* **45,** 494–497 (1980).
2. Tsui, D. C., Stormer, H. L. & Gossard, A. C. Two-dimensional magnetotransport in the extreme quantum limit. *Phys. Rev. Lett.* **48,** 1559–1562 (1982).
3. Novoselov, K. S. *et al.* Two-dimensional gas of massless Dirac fermions in graphene. *Nature* **438,** 197–200 (2005).
4. Zhang, Y. B., Tan, Y. W., Stormer, H. L. & Kim, P. Experimental observation of the quantum Hall effect and Berry's phase in graphene. *Nature* **438,** 201–204 (2005).
5. Haldane, F. D. M. & Raghu, S. Possible realization of directional optical waveguides in photonic crystals with broken time-reversal symmetry. *Phys. Rev. Lett.* **100,** 013904 (2008).
6. Raghu, S. & Haldane, F. D. M. Analogs of quantum-Hall-effect edge states in photonic crystals. *Phys. Rev. A* **78,** 033834 (2008).
7. Wang, Z., Chong, Y. D., Joannopoulos, J. D. & Soljacic, M. Reflection-free one-way edge modes in a gyromagnetic photonic crystal. *Phys. Rev. Lett.* **100,** 013905 (2008).
8. Prange, R. E. & Girvin, S. M. (eds). *The Quantum Hall effect* (Springer, 1987).
9. Thouless, D. J., Kohmoto, M., Nightingale, M. P. & Dennijs, M. Quantized hall conductance in a two-dimensional periodic potential. *Phys. Rev. Lett.* **49,** 405–408 (1982).
10. Simon, B. Holonomy, the quantum adiabatic theorem, and Berry phase. *Phys. Rev. Lett.* **51,** 2167–2170 (1983).
11. Kohmoto, M. Topological invariant and the quantization of the Hall conductance. *Ann. Phys.* **160,** 343–354 (1985).
12. Haldane, F. D. M. Model for a quantum Hall effect without Landau levels: condensed-matter realization of the ''parity anomaly''. *Phys. Rev. Lett.* **61,** 2015–2018 (1988).
13. Hatsugai, Y. Chern number and edge states in the integer quantum Hall effect. *Phys. Rev. Lett.* **71,** 3697–3700 (1993).
14. Yablonovitch, E. Inhibited spontaneous emission in solid-state physics and electronics. *Phys. Rev. Lett.* **58,** 2059–2062 (1987).
15. John, S. Strong localization of photons in certain disordered dielectric superlattices. *Phys. Rev. Lett.* **58,** 2486–2489 (1987).
16. Joannopoulos, J. D., Johnson, S. G., Winn, J. N. & Meade, R. D. *Photonic Crystals: Molding the Flow of Light* (Princeton Univ. Press, 2008).
17. Chong, Y. D., Wen, X. G. & Soljacic, M. Effective theory of quadratic degeneracies. *Phys. Rev. B* **77,** 235125 (2008).
18. Pozar, D. M. *Microwave Engineering* 2nd edn (Wiley, 1998).
19. Murakami, S., Nagaosa, N. & Zhang, S.-C. Dissipationless quantum spin current at room temperature. *Science* **301,** 1348–1351 (2003).
20. Kane, C. L., Mele, E. J. & Z. (2) topological order and the quantum spin Hall effect. *Phys. Rev. Lett.* **95,** 146802 (2005).
21. Bernevig, B. A., Hughes, T. L. & Zhang, S. C. Quantum spin Hall effect and topological phase transition in HgTe quantum wells. *Science* **314,** 1757–1761 (2006).
22. Hsieh, D. *et al.* A topological Dirac insulator in a quantum spin Hall phase. *Nature* **452,** 970–975 (2008).
23. Moore, J. E., Ran, Y. & Wen, X.-G. Topological surface states in three-dimensional magnetic insulators. *Phys. Rev. Lett.* **101,** 186805 (2008).
24. Yu, Z. F. & Fan, S. H. Complete optical isolation created by indirect interband photonic transitions. *Nature Photon.* **3,** 91–94 (2009).
25. Baba, T. Slow light in photonic crystals. *Nature Photon.* **2,** 465–473 (2008).
26. Thevenaz, L. Slow and fast light in optical fibres. *Nature Photon.* **2,** 474–481 (2008).
27. Povinelli, M. L. *et al.* Effect of a photonic band gap on scattering from waveguide disorder. *Appl. Phys. Lett.* **84,** 3639–3641 (2004).
28. Pendry, J. B., Holden, A. J., Robbins, D. J. & Stewart, W. J. Magnetism from conductors and enhanced nonlinear phenomena. *IEEE Trans. Microw. Theory Tech.* **47,** 2075–2084 (1999).
29. Yen, T. J. *et al.* Terahertz magnetic response from artificial materials. *Science* **303,** 1494–1496 (2004).
30. Linden, S. *et al.* Magnetic response of metamaterials at 100 terahertz. *Science* **306,** 1351–1353 (2004).

Supplementary Information is linked to the online version of the paper at www.nature.com/nature.

Acknowledgements We are very grateful to P. Fisher and U. J. Becker for generously providing access to the synchrotron magnet at Massachusetts Institute of Technology. We should like to thank I. Chuang, P. Bermel, J. Bravo-Abad, S. Johnson and P. Rakich for comments. This work was supported in part by the Materials Research Science and Engineering Program of the US National Science Foundation under award number DMR-0819762, and also in part by the US Army Research Office through the Institute for Soldier Nanotechnologies under contract no. W911NF-07-D-0004.

Author Contributions Z.W., Y.C, J.D.J and M.S. designed the photonic-crystal system, analysed the data and wrote the manuscript. Z.W. and Y.C. fabricated the structure and performed all the experimental measurements.

Author Information Reprints and permissions information is available at www.nature.com/reprints. Correspondence and requests for materials should be addressed to Z.W. (zhwang@mit.edu).

METHODS

Parallel-plate waveguide for out-of-plane confinement. The unidirectional CES waveguide was designed to reproduce the dispersion relation and the modal profile of a topological edge mode of a 2D gyromagnetic photonic crystal, using a 3D structure with a finite height. The out-of-plane confinement in the z direction was achieved using two parallel horizontal copper plates, separated by 7.0 mm. This structure is known as a parallel-plate waveguide in microwave engineering[18]. It supports TEM modes with electric fields pointing in the out-of-plane z direction and magnetic fields parallel to the x–y plane. This polarization is identical to the TM modes in 2D photonic crystals where topological modes have been proposed to exist[7]. Between the two plates, the electromagnetic fields of TEM modes are also uniform along the z direction, as in a 2D system. This 3D structure therefore closely mimics a 2D system and is considered to be quasi-2D. When operated below 21 GHz, the waveguide supports only TEM modes.

Single-mode microwave CES waveguide and absorbing boundaries. Similar to the case of conventional waveguides, if the edge waveguide has too large a cross-sectional area it could lead to multimode operation, causing both a unidirectional CES as well as conventional bidirectional modes to be present in the waveguide. To ensure that only a CES is present in the measurement set-up, we chose the distance between the photonic crystal and the conducting copper wall to be 25 mm, which is narrow enough to eliminate all bidirectional modes at the frequencies of the second band gap. With a 6% relative bandwidth for this band gap, a CES is confined within three lattice constants of the edge, even around a large scatterer. The copper scatterer had a height of 7.0 mm and a width of 7.2 mm, with its maximum length mainly limited by the finite size of the crystal used in this experiment. Microwave-absorbing foam pieces were placed along the other three edges of the photonic crystal, to prevent the CES from circulating all the way around the boundary of the crystal. In addition, these foam pieces shielded the system from external interference.

Microwave transmission measurement for bulk crystals and for CESs. Two identically constructed antennas were inserted through the top copper plate, extending to contact the bottom copper plate. These antennas, labelled A and B in Fig. 1a, were connected by coaxial cables to the two ports of a Hewlett Packard 8719C vector network analyser, which measures the transmission coefficients S_{AB} and S_{BA}. Two-port short–open–load–through calibrations were performed at the coaxial adaptor. Therefore, measured S parameters contain a frequency-dependent insertion loss from the impedance mismatch between the antenna, the feed coaxial cable and the photonic-crystal waveguide, and from the transition between the balanced parallel plates and the unbalanced coax cable. This loss is reciprocal and does not affect the ratio of the transmission coefficients, $|S_{AB}/S_{BA}|$. Therefore, any substantial difference between $|S_{AB}|$ and $|S_{BA}|$ is an experimental signature of the unidirectionality of CESs. We extracted the forward and backward transmission spectra in a frequency sweep from 1 to 6 GHz. Each measurement was performed with an intermediate frequency of 20 Hz and four averages, with the power level normalized to the level at the band edges. To measure bulk band gaps (Fig. 3a), antennas A and B were located along the long axis of a 16×10 photonic crystal, eight lattice constants apart (Supplementary Information). For the CES waveguide (Figs 3c and 4), we performed the measurement with the feed and probe antennas located between the copper wall and the 16×7 photonic crystal, also eight lattice constants apart (Fig. 1a), and with the metal wall 9 mm away from each antenna.

Effects of material absorption loss. Most of the propagation loss in the present system may be attributed to two sources: the radiation losses originating from the finite width of the photonic-crystal cladding and the intrinsic material absorption associated with the ferromagnetic resonance. The radiation loss could be further reduced simply by increasing the number of unit cells in the lateral direction, whereas the absorption loss could in principle be further reduced by using monocrystalline yttrium–iron-garnet as the ferrite material[18]. The resultant attenuation length would be on the order of hundreds of lattice constants.